16th Australasian Fluid Mechanics Conference
Crown Plaza, Gold Coast, Australia
2-7 December 2007

Comparison of drag measurements of two axisymmetric scramjet models at Mach 6

Katsuyoshi Tanimizu, D. J. Mee and R. J. Stalker

Division of Mechanical Engineering
University of Queensland, Queensland Australia, 4072 AUSTRALIA

Abstract

Axial forces on quasi-axisymmetric scramjet models designed for operation at Mach 6 and Mach 8 were measured in the T4 Stalker tube at The University of Queensland using a single component stress wave force balance. A Mach 6 nozzle was used. The nozzle supply enthalpy was varied from 3 to 9 MJ/kg and the nozzle supply pressure from 35 to 45 MPa. As the conditions varied, the Mach number varied from 5.7 to 6.7. For both test models, the drag coefficients decreased with increasing Mach number. However, significant differences between the models were not observed over a range of free stream Mach numbers. A theoretical procedure to calculate the drag coefficient was found to give good agreement with experiments when appropriate account was taken of flow spillage at the intake.

Nomenclature

A	Model frontal Area, m^2
C_D	Drag Coefficient
C_{TN}	Coefficient of thrust
D	measured axial force, N
U	free stream velocity, m/s
ΔQ	heat released by fuel combustion in air
γ	ratio of specific heats
f	calibration factor
$u(t)$	single input to the system
$y(t)$	output from the system
$g(t)$	impulse response function from the system
p_p	Pitot pressure, kPa
p_s	nozzle supply pressure, MPa

Introduction

In the case of propulsion, the attractive potential of hypersonic flight with an air-breathing engine within atmosphere has been appreciated for past 50 years. A vehicle which uses a scramjet engine is a major candidate for future spacecraft and hypersonic planes. There are still many difficulties encountered in developing hypersonic planes. Unlike rocket engines, scramjet engines are air breathing. This means that scramjet engines do not need to carry oxidizer to burn fuel and produce thrust. Since a rocket is not air-breathing, its oxidizer must be carried on board. However, most of the oxidizer is burned up before the rocket exits the atmosphere. Using air breathing engines in the atmosphere can reduce the amount of oxidizer carried by the vehicle. That means larger payloads can be launched into space for a given take-off mass.

In 2002, The University of Queensland conducted the first successful scramjet flight experiment [1]. Two years later, NASA's X-43A demonstrated that an air-breathing engine (a scramjet engine) could fly at nearly 10 times the speed of sound. The success of these flight tests will hopefully lead to an operational hypersonic air breathing vehicle in the near future.

About fifteen years ago in the Centre for Hypersonics at The University of Queensland measurements were made of the axial force on a quasi-axisymmetric scramjet model in the T4 Stalker tube. At some test conditions, a positive net thrust was measured using a silane-hydrogen fuel [2]. Analysis indicated that the performance of the quasi-axisymmetric scramjet could improve if a more effective aerodynamically designed nozzle was used. However, since the engines on scramjet-powered vehicles are integrated into the vehicle design, changing the nozzle usually cannot be done without changing other parts of the vehicle.

The thrust of a scramjet powered-vehicle is analyzed by Stalker [3]. He relates the thrust coefficient to the heat release due to combustion of the fuel, the flight speed and the drag coefficient,

$$C_{TN} = (2\Delta Q/U^2)(1 - 0.5\Delta Q/U^2) - C_D. \quad (1)$$

Stalker notes that *"$C_{TN} = 0$ for a vehicle in the cruise phase, while for a vehicle in the boost phase, C_{TN} forms a product with the flight velocity which is proportional to the net fuel specific impulse, and therefore is a measure of the efficiency with which fuel is used in acquiring vehicle velocity."*[3]

Equation (1) clearly shows that reducing the drag force on a scramjet-powered vehicle is very important in improving the overall performance of the vehicle.

The main purpose of this paper is to investigate the effect of the combustion chamber and the nozzle geometry on the overall performance of a scramjet model by quantifying axial forces.

Test models and measurement method

T4 Stalker tube

Experiments were conducted in the T4 free piston shock tunnel at The University of Queensland. In this study, the Mach 6 nozzle was used. This shock tunnel can produce suitable flows for scramjet research. It consists of a reservoir, a compression tube which is 26 m long, a shock tube which is 10 m long, and a test section. The compression tube and the shock tube are separated by the primary diaphragm. The shock tube has three timing stations each 2.05 m apart. These are used to measure the speed of the shock wave in the shock tube. There are two pressure transducers mounted at the end of the shock tube. These are used to measure the nozzle supply pressure. The nozzle supply pressure was approximately 35 to 45 MPa in this test campaign. The nozzle supply enthalpy was varied from 3 MJ/kg to 9 MJ/kg. For the current tests the test gas was air. The compression tube was filled with a mixture of argon and helium. The nozzle supply pressure, test gas temperature and shock speed were measured and used to determine the test flow conditions. The end of the test time was determined either by when the test gas was estimated to have been contaminated by more than 10% by the driver gas, or when the nozzle supply pressure dropped 10% below the mean value of the nozzle supply pressure after the nozzle starting process had been completed.

Test models

Figure 1 (a) shows the quasi-axisymmetric scramjet models used in the present study. These scramjets were designed by Prof. R. J. Stalker. The top half of Fig. 1 (a) is the quasi-axisymmetric scramjet model designed for Mach 6 flow condi-

tions. This is referred to as model 1. It was directly developed from that used in Paull et al.[2], and has a 9° half-angle conical forebody, and 10° half-angle conical afterbody. The inlets and combustion chamber entrances consist of compression ramps formed by six splitters which deflect the flow that has already passed through the conical forebody by a further 8.0°. Constant area combustion chambers are formed by the centrebody, the cowl, and the splitters which are 60 mm long. Expansion nozzles are formed by the afterbody , the cowl and the splitters which have a 10° deflection angle. The bottom half of Fig. 1 (a) is the quasi-axysmmertic scramjet designed for Mach 8 flow conditions. This is referred to as model 2. This scramjet model also consists of an axisymmetric centrebody, with six combustion chambers, associated intakes, thrust nozzles, and a cowl. The intake, combustion chamber, and thrust nozzle are symmetrically arranged on an axisymmetric centrebody. The centrebody consists of a 9° half-angle conical forebody, and a 4° and 11.3° half-angle conical afterbody. The internal intakes are formed by six 9° wedges and the cowl. The combustion chambers are bounded by side walls, a conical afterbody of 4° half-angle, and the cowl. A 4° expansion in the combustion chambers was chosen to prevent the flow from choking. The length of the combustion chambers is 30 mm. At the downstream end of the combustion chamber, the splitters deflect the flow through an angle of 7.6°. The 11.3° half-angle conical afterbody forms the inner surface of the thrust nozzles. The trailing edge of the cowl also deflects the flow by 6° from the incoming stream direction.

(a) Photographs of model 1 (top) and model 2 (bottom)

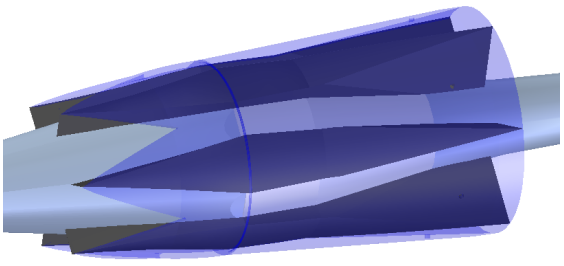

(b) CAD drawing of model 2 enlarged intake area. Note that the cowl is shown as being translucent so that the internal geometry can be seen.

Figure 1: The test models

Force measurement method

A single component stress wave force balance was applied to measure the axial aerodynamic forces on the models. This technique involves measuring stress waves which propagate and reflect through the model and the stress bar [4]. The dynamic

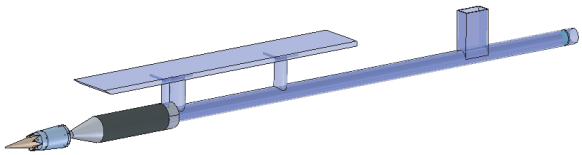

Figure 2: Test model assembly

behaviour of the model and stress bar combination may be analytically modelled as a time invariant, linear system described by the convolution integral (Eq. 2),

$$y(t) = \int_0^t g(t-\tau)u(\tau)d\tau. \quad (2)$$

The unit impulse response function was obtained through calibration using a PCB piezotronics impulse force hammer (Model No. 086C04). A schematic diagram of the assembly of the test model and support structure is shown in Fig. 2. A fuel tank and a fast acting valve were mounted behind the model. (Note however that no fuel was injected in the current tests.) A 2 m long stress bar was connected to the fuel tank. Four piezo-electric film strain gauges were installed on the bar. The signal from only one gauge is required to determine the drag force, however, signals from all four gauges were used to determine the force on the model. The signals determined from each of the four gauges were then averaged to produce a force signal. The test model and the stress bar were suspended by two thin wires. These wires ensured that the model and the stress bar were free to move during the test time. The stress bar, the fuel tank and the fast acting valve were enclosed in aerodynamic shielding in order that the aerodynamic force only acts on the test model.

Flow visualization method

Flow visualizations on the conical forebody and intake were conducted using the Background Oriented Schlieren method (BOS) [5]. The BOS system is a simple but effective method for visualization of compressible flow. The BOS system needs only a digital camera to record two images of a pattern located behind the flow of interest, a light source, and a background pattern. One photograph is taken when there is no flow and another with flow. The differences between the images are used to infer differences in the refractive index of the medium between the camera and the pattern. An in-house code ”bos-GUI” was used for image processing [6].

Force measurements

An example of the measured drag signal obtained for Shot 9376 is shown in Fig. 3. Shot 9376 had a nozzle supply pressure of 35 MPa, nozzle-supply enthalpy of 4.0 MJ/kg and a free stream Mach number of 6.3. The strain signals were not zero at the start of the test time due to low frequency oscillations generated by tunnel movement transmitted to the sting through the support wires. The zeros of the raw strain signals were adjusted before the signals were deconvolved. The four raw strain outputs were deconvolved with the impulse response functions determined in the calibration tests and then averaged. Figure 3 indicates the drag force on the test model during test time. For this shot, the drag force during the test time (8.0 to 9.1 ms) was 170 N.

The drag force was used with the test flow conditions to calculate the drag coefficient. In this study the drag coefficient, C_D, was calculated from the measured drag force, D, and the pitot pressure, p_p, (see Mee[7]). This method takes into account any fluctuations in the test flow during the test time. The pitot pressure could not be measured reliably because of the limited size

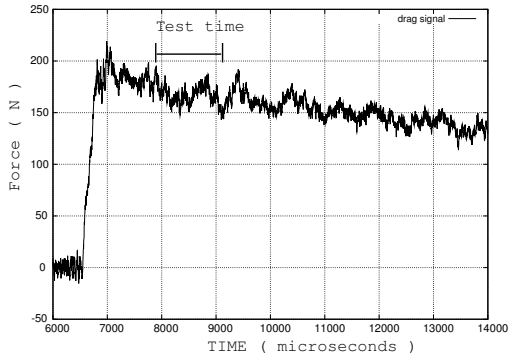

Figure 3: Deconvolved drag force signal for Shot 9376

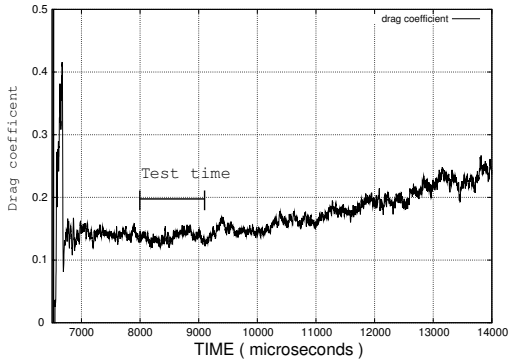

Figure 4: The measured drag coefficient shot No. 9376

of the nozzle core flow and the size of the test model. However, once the nozzle flow has become established, experiments in T4 show that the Pitot pressure signal follows the nozzle supply pressure signal. The Pitot pressure is then a constant factor times the nozzle-supply pressure. Therefore, the measured nozzle-supply pressure signal was used to determine the variation in Pitot pressure during the test period for the present experiments. The Pitot pressure was calculated as $p_p = f p_s$, where p_s is the measured nozzle supply pressure. The factor, f, used in this study was 0.012. The final expression used to calculate C_D was

$$C_D = \left[\frac{2}{(\frac{\gamma+1}{2})^{\frac{\gamma+1}{\gamma-1}} \gamma^{\frac{\gamma}{\gamma-1}} A} \right] \frac{D}{f p_s}, \qquad (3)$$

The drag coefficient for shot 9376 is shown in Fig. 4. The drag coefficient during the test time (8 to 9.1 ms) is approximately 0.15.

Analysis of performance

This section describes the theoretical modelling used to estimate the drag force on the axisymmetric scramjet in the absence of fuel injection using simple hypersonic theories. Drag is produced by the tangential (skin friction) and normal (pressure) forces acting on the scramjet model. The total drag force has been calculated for each component separately.

Force on the cone

Both scramjet forebodies consist of a 9° half-angle cone. As a result, a conical shock wave is generated at the tip of the cone. This shock wave produces a uniform pressure on the cone surface. The uniform pressure on the cone surface was calculated using the theory of Taylor and Maccoll [8]. The pressure force on the conical forebody was calculated by multiplying the cone surface area by the predicted cone surface pressure. The skin friction drag on the conical forebody was calculated using a laminar reference temperature method [9]. When the Reynolds number became larger than the transition Reynolds number, the boundary layer was assumed to be turbulent. He and Morgan's [10] T4 shock tunnel test results were used in this study to estimate the transition Reynolds number for different unit Reynolds numbers. The theory of van Direst[11] was used to calculate the turbulent skin friction drag.

Force on the intake

The internal inlets of the scramjet model were formed by the splitters, the conical forebody and the cowl. The splitters were machined so that the splitter's surface is always normal to the cone surface. Therefore, it was assumed that the oblique shocks generated at the leading edges of splitters were also normal to the cone surface, and uniform pressures were created by oblique shocks. The boundary layer on the internal intake was assumed to be laminar for all conditions, except when the Reynolds number reached the transition Reynolds number, then the boundary layer was assumed to be turbulent.

Force on the cowl

In order to simplify the calculations, the pressures on the external surface of the cowl were calculated using two-dimensional planar shock wave and expansion theories. For the 6° expansion on the cowl, Prandtl-Meyer expansion theory was applied to find the flow conditions. In determining the skin friction on the external surfaces of the cowl, the boundary layer on the cowl was assumed laminar. However, when the Reynolds number reached the transition Reynolds number, the boundary layer was assumed to be turbulent.

Force on the combustion chamber and nozzle

The forces on the combustion chamber and nozzle of each model were computed using an in-house CFD three dimensional Navier-Stokes equation solver, "Elmer" [13]. In order to reduce the calculation time, skin friction drag was calculated separately. That is, Elmer was used to calculate only the inviscid forces on the combustor and nozzle surfaces. The surface pressures calculated using Elmer at all locations were extracted and used to calculate the inviscid drag. The skin friction drag in the combustion chamber and the nozzle were computed using the theory of van Direst[11] with conditions outside the boundary layer taken from the Elmer simulations. The pressure and Mach number used to compute forces on the combustion chamber and the nozzle were found using an adiabatic stream tube relation including entropy changes across shock waves [12].

Experimental results

The results of M6 flow

The drag coefficients on the axisymmetric scramjet models at Mach 6 flow conditions are plotted as a function of free stream Mach number in Fig. 5. The theory and the experiment results show the same trends. However, there are significant differences between the theory and the experiment for model 2. This is attributed to the fact that, at the Mach 6 flow condition, the conical shock wave was not captured completely by the cowl. A BOS image of the flow around model 2 is shown in Fig. 6. For this condition, the free stream Mach number was 6.2 and nozzle supply enthalpy was 5.8 MJ/kg. As can be seen, the conical shock wave generated at the cone tip was not captured. An oblique shock wave can also be seen generated at the crotch of the cowl.

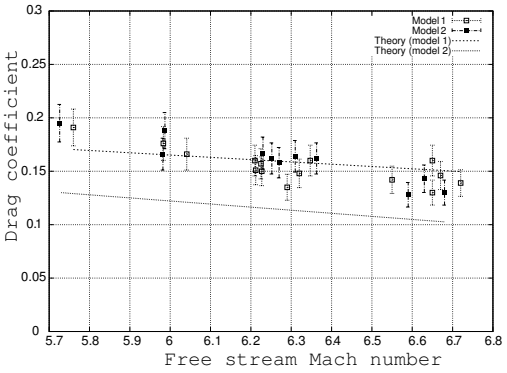

Figure 5: The results of Mach 6 flow conditions

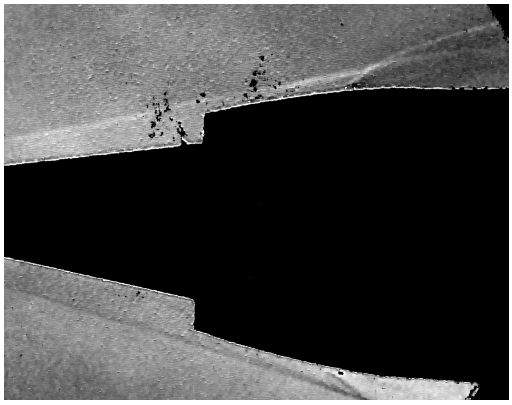

Figure 6: BOS picture of the model 2 , shot No 9417, 5.8 MJ/kg

Therefore, some compressed flow was spilt outside the cowl. This spillage affects the total performance of model 2. However, large differences in C_D between model 1 and model 2 were not observed in experiments.

The effect of spillage is that less flow is captured by the intake than was assumed in the theoretical model. Therefore an adjustment was made to the theoretical model. The actual capture area was calculated by tracing streamlines between the model surface and the conical shock wave. The streamline traces were calculated by solving the Taylor and Maccoll equations as detailed by Anderson [14].

The flow that enters the intake was found by tracing the streamline that just hits the edge of the intake. Mass below this line enters the scramjet combustor and mass above it spills. The theoretical calculation results including the spillage effect are shown in Fig. 7. As can be seen, the theoretical results using the corrected model show much better agreement with the experiment results. Figure 8 shows a break-down of the calculated drag coefficient for model 1 and 2 at three free stream Mach numbers. Note that although the overall drag coefficients for the two models are similar, the break-down is very different. The pressure and skin friction drag decrease with increasing free stream Mach number for both models. The pressure drag of model 2 was larger than that of model 1 because of the larger pressure drag on the conical forebody, and the larger internal intake of model 2. The thrust coefficient of model 2 was larger than that of model 1 because the internal compression provided higher pressures in the combustion chambers. The skin friction drag coefficient did not differ significantly between two models.

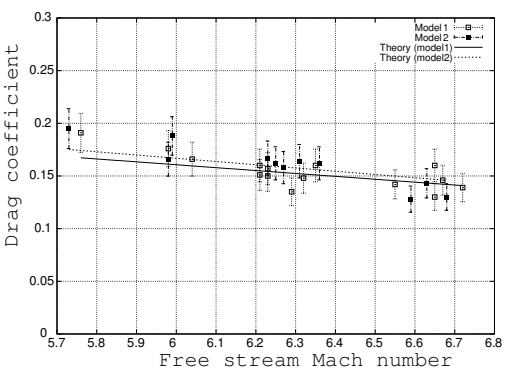

Figure 7: The results of Mach 6 flow conditions

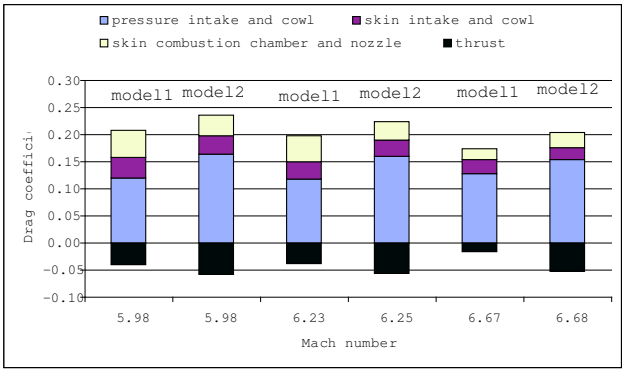

Figure 8: Drag coefficient break-down for Model 1 and 2

Conclusions

Experiments to measure the axial force on two differently shaped quasi-axisymmetric scramjet models were conducted. The theoretical calculations were generally in good agreement with the experimental results. Spillage drag had a significant effect on the total performance of the model. Significant differences in the overall drag coefficient for the two models were not observed at these Mach 6 flow conditions.

Acknowledgements

The authors would like to thank of James Turner, Andrew Ridings, Sarah Razzaqi, and Thomas Jazra for their assistance in the during the experiments. Thanks also to Keith Hitchcock for modifications to the test models and Dwishen Ramanah for setting up the visualization system. Finally, the authors would like to thank Dr. Peter Jacobs for assistance with building the CFD model. This work was supported by the Australian Research Council through Discovery Project DP0452374.

References

[1] Smart,M, K. and Hass, E, N. and Paull, A., *Flight Data Analysis of the HyShot 2 Scramjet Flight Experiment*, AIAA Journal, Vol 44, No. 10, October 2006, pp.2366 - 2375.

[2] Paull, A. and Mee, D. J. and Stalker, R. J., *Experiments on supersonic combustion ramjet propulsion in a shock tunnel*, Journal of Fluid Mechanics, Vol 296, 1995, pp. 159 - 183.

[3] Stalker, R. J. and Paull, A. and Mee, D. J. and Morgan, R. G. and Jacobs, *Scramjets and shock tunnels - The Queens-*

land experience, Progress in Aerospace Sciences, Vol. 41, 2005, pp. 471 - 513.

[4] Sanderson, S. R. and Simmons, J. M., *Drag balance for hypervelocity impulse facilities*, AIAA Journal, Vol. 29, No. 12, 1991, pp. 2185 - 2191.

[5] Ramanah, D. and Raghunath, S. and Mee, D, J. and Rösgen, T. and Jacobs A, P., *Background oriented schlieren for flow visualisation in hypersonic impulse facilities*, Shock Waves, Vol. 17, 2007, pp. 65 - 70.

[6] Ramanah, D., *Background Oriented Schlieren Technique for Flow Visualization in Shock Tunnels*, Mphil thesis, The University of Queensland, Division of Mechanical Engineering, (submitted), 2007.

[7] Mee, D. J., *Dynamic calibration of force balances*, Division of Mechanical Engineering, The University of Queensland, Research Report 2002/6, 2002

[8] Taylor, G, I. and Maccoll, W, J. *The air pressure on a cone moving at high speed*, Proceedings of the Royal society of London, Series A, Vol. 139, No. 838, 1933, pp. 278 - 297.

[9] Simeonides, G., *Generalized reference enthalpy formulations and simulation of viscous effects in hypersonic flow*, Shock Waves, Vol. 8, No. 3, 1998, pp. 161 - 172.

[10] He, Y., and Morgan, R. G., *Transition of compressible high enthalpy boundary layer flow over a flat plate*, Aeronautical Journal, Vol. 98, No. 25, February 1994, pp. 25 - 34.

[11] van Driest, E. R., *Problem of Aerodynamic Heating*, Aeronautical Engineering Review, Vol. 15, No. 10, 1956, pp. 26 - 41.

[12] Hall, A, N., *Thermodynamics of Fluid Flow*, Prentice-Hall, ING, 1951, pp. 112 - 113.

[13] Jacobs, P., *Computer program "Elmer" - a 3-D Navier-Stokes equation solver*, 2006 (Private communication).

[14] Anderson, D, J., *MODERN COMPRESSIBLE FLOW with Historical Perspective*, McGRAW-HILL, INC, 1990, pp. 301 - 305.